Magnetic phase diagram of fcc disordered $Ni_{1-x}[Fe(Mn)]_x$ alloys

A. Z. Men'shikov, A. E. Teplykh, and V. I. Kuznetsov

Institute of Metal Physics, Ural Branch of the Academy of Sciences of the USSR
(Submitted 25 October 1990)
Zh. Eksp. Teor. Fiz. **99**, 1772–1783 (June 1991)

Since it is not possible to construct the magnetic phase diagram of γ-$Ni_{1-x}Fe_x$ alloys, because of the $\gamma \rightarrow \alpha$ structural phase transition, we have undertaken in the present work the replacement of iron by manganese atoms for $x > 0.7$. For this purpose the magnetic phase diagram of the quasibinary section of $Fe_{0.7}Ni_{0.3-c}Mn_c$ has been studied in detail by neutron diffraction, magnetic measurements and by Mössbauer spectroscopy. It is shown that there are two tricritical points on the combined phase diagram of γ-$Ni_{1-x}[Fe(Mn)]_x$ which separate regions of homogeneous ferromagnetism from inhomogeneous (frustrated) magnetism, while in the region of the critical concentration for long-range order a spin-glass state is realized involving short-range magnetic correlation.

Alloys of the $Ni_{1-x}Fe_x$ system, forming the basis of a large group of industrially important materials with special magnetic, thermal and elastic properties, belong to typical disordered systems with competing exchange interaction of the type $J_{NiNi} > 0$, $J_{NiFe} > 0$ and $J_{FeFe} < 0$ (Refs. 1,2). Their magnetic state for different temperatures is of interest both for unravelling the Invar problem and also for constructing a complete magnetic phase diagram reflecting the evolution of a concentration phase transition from homogeneous ferromagnetism to homogeneous antiferromagnetism within the limits of fcc symmetry of the crystal lattice of magnetic atoms.

Attempts have been made more than once in the literature[3–5] to construct such a diagram, but because of the existence of the structural $\gamma \rightarrow \alpha$ transformation in this system at $x \approx 0.7$ it was not possible to trace the complete transition from ferromagnetic long-range order to antiferromagnetic and to establish the nature of the magnetic states in the intermediate region. In order to show, somehow, a possible type of phase diagram for $Ni_{1-x}Fe_x$ alloys, characterized by a fcc lattice, over the whole composition range, the method of replacing iron by manganese atoms for $x = 0.7$ was used. As is well known,[6,7] manganese atoms, unlike iron atoms, stabilize the γ-phase in this concentration region and an alloy of the composition $Fe_{0.7}Mn_{0.3}$ has a collinear antiferromagnetic structure with a wave vector $\mathbf{k} = (2\pi/a)(1,0,0)$.[8]

It is evident that the replacement of iron by manganese atoms is not equivalent from the point of view of the magnitude of the exchange interaction of the atoms, but the sign of this interaction stays the same, since according to Menshikov *et al.*[9] $J_{FeFe} \approx -9$ meV, $J_{MnMn} \approx -285$ meV, $J_{NiFe} \approx 38$ meV, $J_{NiMn} \approx 44$ meV, $J_{FeMn} \approx 17$ meV.

In order to realize this idea it was necessary to study, in addition to the previously studied $Ni_{1-x}Fe_x$ alloys,[3–5] the system of quasibinary solid solutions corresponding to the formula $Fe_{0.7}Ni_{0.3-c}Mn_c$. The fixed iron concentration ($x = 0.7$) was chosen from the the considerations that, on the one hand, it is close to the critical concentration $x_F = 0.75$ for the existence of long-range ferromagnetic order in $Ni_{1-x}Fe_x$ alloys, and, on the other, it avoids the structural $\gamma \rightarrow \varepsilon$ transformation which occurs in iron-manganese alloys with iron content greater than 70 at. %. The magnetic state of γ-$Fe_{0.7}Ni_{0.3-c}Mn_c$ alloys was established by the methods of elastic scattering of neutrons, magnetic measurements and γ-resonance spectroscopy.

EXPERIMENTAL METHOD

For the investigations 15 alloys of the quasibinary section of $Fe_{0.7}Ni_{0.3-c}Mn_c$ were melted from chemically pure elements in a purified argon atmosphere, with the manganese concentration varied from 0 to 0.3 (the corresponding manganese concentrations in at. % are shown on the figures in the present work). According to chemical analysis the departure from the specified composition was less than 0.2 at. % in any of the given components.

Before preparing the specimens, ingots were forged in advance into ≈ 10 mm diameter rods which then underwent homogenizing annealing in a helium atmosphere at 1300 K for 100 h. Specimens in the form of cylinders 50 mm long with diameter 6 mm were machined from the billets for the neutron diffraction studies and in the form of disks 0.5 mm thick with 6 mm diameter for the magnetic measurements. Mössbauer studies were carried out on 20 μm thick foils obtained by cold rolling.

The neutron diffraction studies were made on a diffractometer fixed to one of the horizontal channels of the IVV-2M reactor. A germanium single-crystal with (111) reflection plane was used to obtain a monochromatic neutron beam with wavelength $\lambda = 0.181$ nm. Both coherent scattering in the angular range $2\theta = 2$–$80°$ and incoherent small-angle neutron scattering up to the minimum momentum transfer $q = 0.9$ nm^{-1} were studied. Measurements were carried out in the temperature interval 4.2–500 K.

The magnetic properties of the alloys were studied with a vibration magnetometer in fields up to 1.6×10^6 A/m at temperatures from 4.2 to 300 K. The temperature of the specimen was measured with a Cu(Fe)–Cu thermocouple with an uncertainty of ± 1 K. The relative uncertainty in the magnetization measurements was less than 2%.

The study of the Mössbauer spectra was carried out on a NP-255 spectrometer in the temperature range 4.2–300 K. The γ-quanta source was a Co(Pd) specimen of activity ≈ 0.7 Bq. A gas-filled proportional counter with energy resolution $\Delta E \approx 15\%$ was used as detector. The chemical shifts were calculated relative to α-Fe. The spectra were analyzed with a SM-4 computer using the least-squares method.

 0038-5646/91/060991-07$03.00

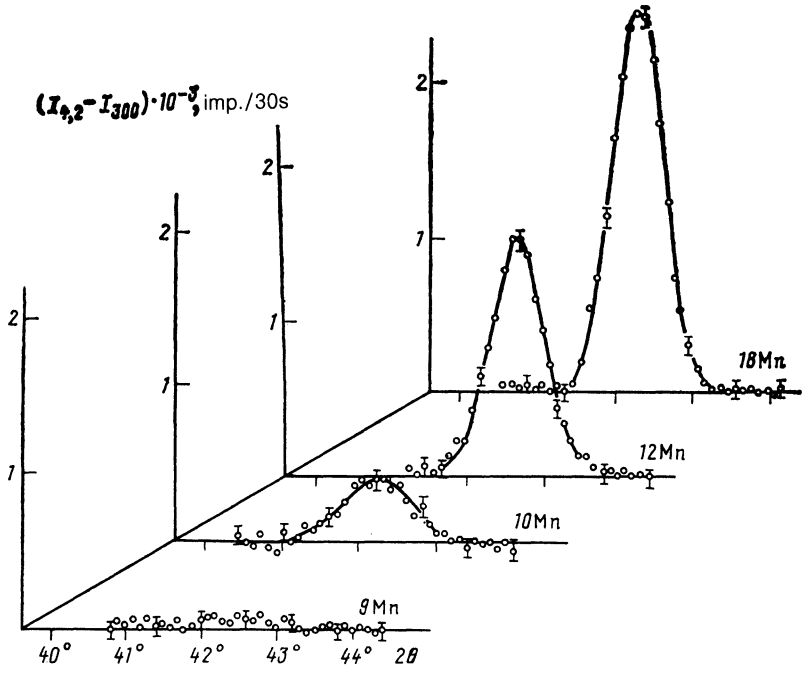

FIG. 1. Change in intensity of the (110) magnetic reflection in $Fe_{0.7}Ni_{0.3-c}Mn_c$ alloys in the vicinity of the critical concentration c_{AF} for the disappearance of long-range antiferromagnetic order.

EXPERIMENTAL RESULTS AND DISCUSSION

Neutron diffraction studies. Specimens of the alloys studied were investigated in advance by x-ray diffraction at room temperature and it was found that all the alloys had the fcc structure with lattice parameter varying from $a = 0.3564$ nm for alloys not containing manganese (OMn) to $a = 0.3597$ nm for alloys containing 30 at. % manganese (30 Mn). However, as the temperature decreased, alloys with concentrations $c = 0$ and $c = 0.02$ partially transformed into the α-phase, becoming a spatial two-phase mixture with fcc and bcc structures.

Magnetic fine-structure reflections with indices (110), (210) and (211) were found in the neutron diffraction pictures obtained at 4.2 K of alloys containing 12% manganese and more, pointing to the existence of long-range antiferromagnetic order with wave vector $\mathbf{k} = (2\pi/a)(1,0,0)$. The intensity of the magnetic reflections then decreased on approaching the critical concentration for the existence of long-range antiferromagnetic order c_{AF}, while the line width increased. This is seen clearly in Fig. 1, as illustrated in the change of (110) reflection in the region of the critical concentration. The temperature of the transition to the paramagnetic state was determined from the temperature dependence of the most intense (110) reflection and the mean magnetic moment per atom was calculated from the results on the intensity of magnetic reflections at 4.2 K.

In alloys with concentrations $c < 0.1$ where there are no magnetic reflections a large coherent small-angle neutron scattering (SANS) was found over the whole temperature region of ferromagnetic order (Fig. 2a). However, no critical scattering peak near the temperature of the transition to the paramagnetic state was noted. This peak did not show up even for a three-fold increase in momentum transfer q, as would follow from Fig. 2b, where the temperature dependence of small-angle scattering for the 4Mn alloy is shown. A similar behavior of SANS is characteristic for alloys with inhomogeneous ferromagnetic order, in which there is no

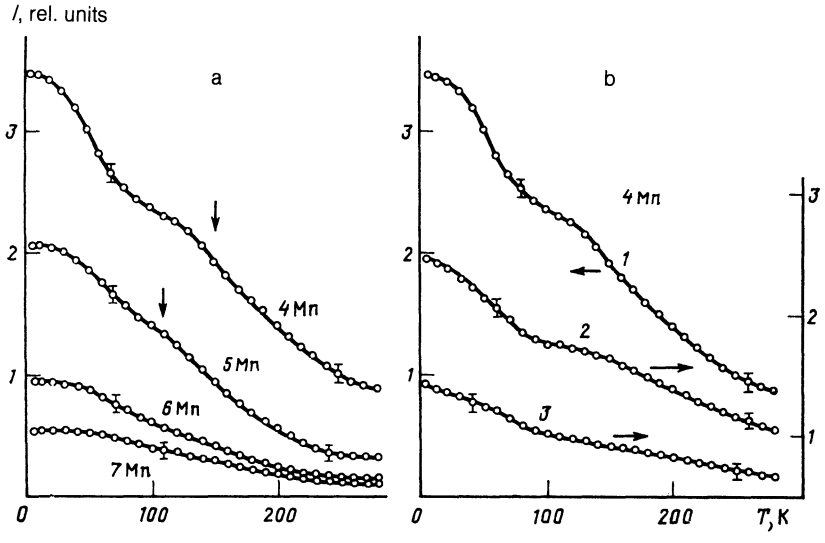

FIG. 2. Temperature dependence of small-angle neutron scattering for $q = 0.9$ nm^{-1} a) for different $Fe_{0.7}Ni_{0.3-c}Mn_c$ alloys and b) for the alloy 4 Mn at different q: 1) 0.9; 2) 2.2; 3) 2.8 nm^{-1}.

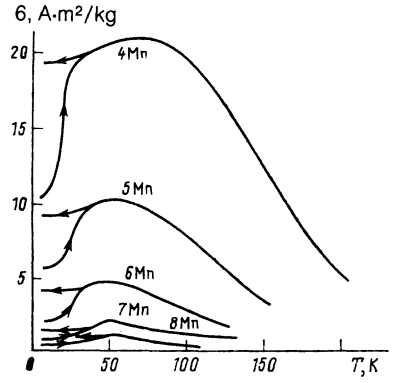

FIG. 3. Temperature dependence of the reversible σ_{FC} (arrow in the direction of increasing temperatures) and irreversible σ_{ZFC} (arrow in the opposite direction) magnetization in $Fe_{0.7}Ni_{0.3-c}Mn_c$ alloys, measured in a field 7.2×10^4 A/m.

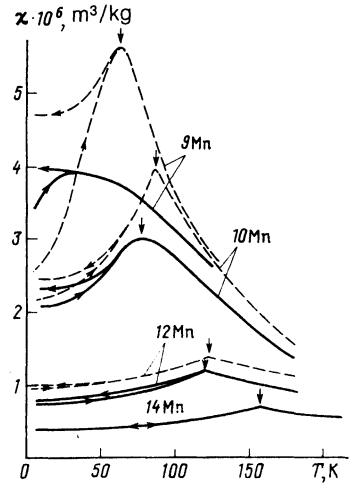

FIG. 4. Temperature dependence of the reversible χ_{FC} (the arrow on a curve in the direction of increasing temperature) and irreversible χ_{ZFC} (arrow in the opposite direction) susceptibility in $Fe_{0.7}Ni_{0.3-c}Mn_c$ alloys, measured in fields 1.6×10^6 A/m (full lines) and 8×10^4 A/m (dashed). Vertical arrows denote the position of T_f.

cooperative character in the ferromagnet–paramagnet phase transition. The growth in SANS as the temperature decreases is also evidence of this. The conditions for the dependence ($T=4.2$ K), put in the coordinates $\ln I=f(\ln q)$ gives a power relation $I\propto q^n$, where n decreases from 3.2 to 2.2 as the manganese content increases from 4 to 7 at. % respectively.

Magnetic properties. Temperature measurements of the magnetization σ (susceptibility χ) were carried out on a specimen cooling in zero magnetic field (ZFC) and in a field corresponding to the measuring field (FC) to determine the magnetic state of alloys in the absence of long-range antiferromagnetic order. As can be seen from Fig. 3, there is irreversibility of the curves $\sigma_{ZFC}(T)$ and $\sigma_{FC}(T)$ for the alloys 4Mn–8Mn, indicating the nonergodicity of the magnetic ground state of these alloys. An irreversibility in susceptibility is also noted for alloys adjacent to the antiferromagnetic region (Fig. 4), where the effects of magnetically coherent neutron scattering are still visible. They occur for all alloys with manganese concentration less than 14 at. %. The $\chi(T)$ curves obtained in different magnetic fields show strong sensitivity to the magnitude of the field, as is seen from Fig. 4. The phenomenon of magnetic viscosity is also present for alloys with magnetic irreversibility, which together with irreversibility of magnetic susceptibility is characteristic for a reentrant phase or a spin-glass state, the transition to which takes place at temperature T_f.

To determine the critical concentration for the disappearance of the ferromagnetic order parameter in the alloys, an analog of the Belov–Arrott method of thermodynamic coefficients was used. For this purpose a family of $\sigma^2=f(H/\sigma)$ curves at 4.2 K was constructed for a number of the alloys studied (Fig. 5) and the critical concentration c_F at which the coefficient $a=0$ in the equation $a+b\sigma^2=H/\sigma$ was determined. As follows from the inset to Fig. 5, in alloys with concentrations $c\leqslant0.055$ the magnetic ground state is characterized by the existence of a ferromagnetic component. The transition temperature of this component to the paramagnetic state was also determined with the help of the method of thermodynamic coefficients because of the absence in these alloys of a step in the $\sigma(T)$ curves obtained in very small fields, characteristic for the kink method.

The method of measuring the temperature dependence

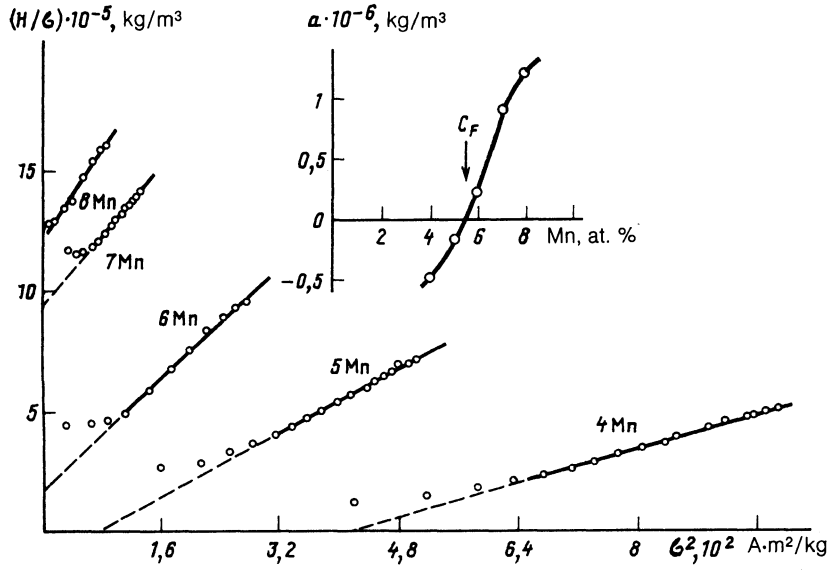

FIG. 5. Dependence of H/σ on σ^2 at 4.2 K for different $Fe_{0.7}Ni_{0.3-c}Mn_c$ alloys. The insert shows how the coefficient a depends on manganese concentration.

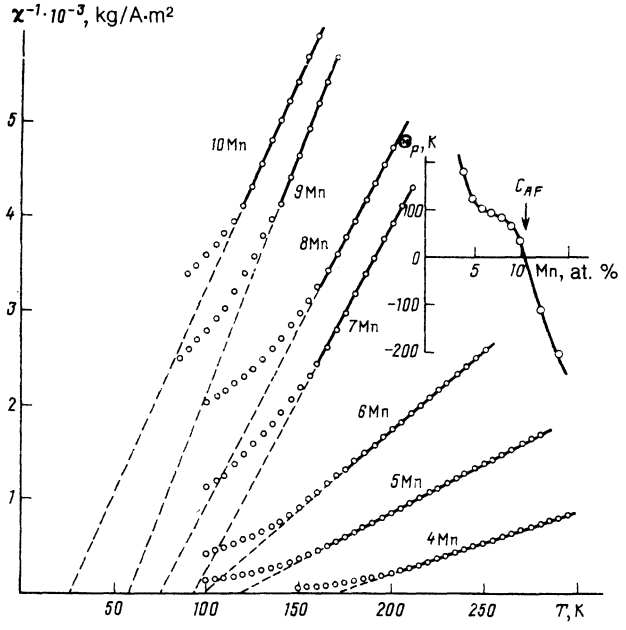

FIG. 6. Temperature dependence of the inverse susceptibility χ^{-1} for $Fe_{0.7}Ni_{0.3-c}Mn_c$ alloys. The inset shows how the paramagnetic Curie point Θ_p depends on the concentration.

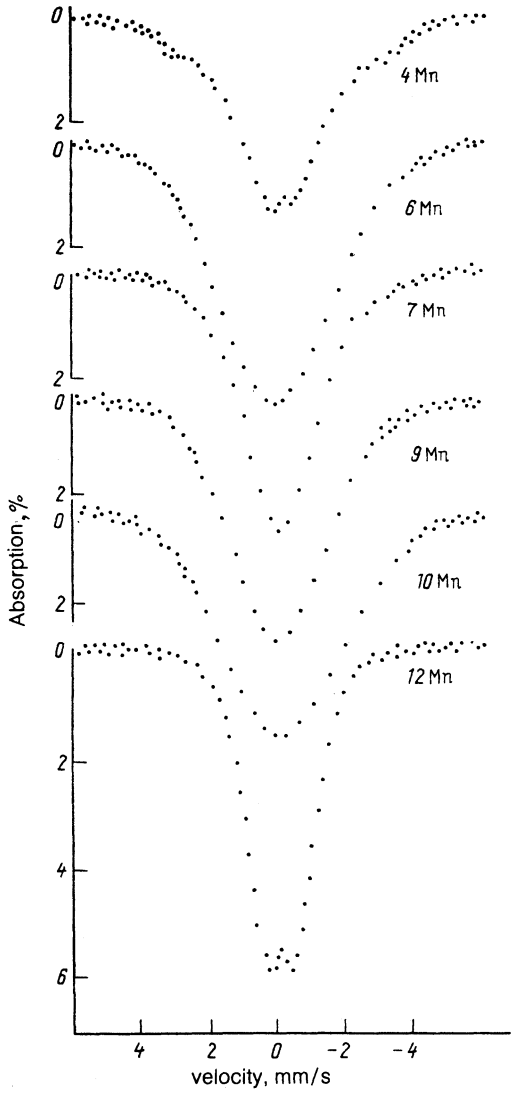

FIG. 7. Mössbauer spectra of $Fe_{0.7}Ni_{0.3-c}Mn_c$ alloys at 4.2 K.

of the magnetic susceptibility $\chi(T)$ in fairly large fields was applied to reveal the critical concentration for the onset of long-range antiferromagnetic order. The low-temperature part of the $\chi^{-1}(T)$ relation is shown in Fig. 6, measured in a field of 7.7×10^5 A/m, the extrapolation of which to $\chi^{-1}=0$ gives the value of the paramagnetic Curie point Θ_p. As can be seen from the concentration dependence of Θ_p, shown in the inset to Fig. 6, $\Theta_p=0$ for the critical concentration $c_{AF}=0.105$. Consequently, in alloys with manganese concentration above c_{AF} the antiferromagnetic interaction is dominant. This fact agrees fairly well with conclusions drawn from the method of elastic scattering of neutrons described above.

Mössbauer studies. In order to reveal the features of the magnetic state of the alloys in the region of the transition from ferromagnetic long-range order to antiferromagnetic the Mössbauer spectra were studied at various temperatures. Their form at 4.2 K is shown in Fig. 7 for alloys containing from 4 to 12 at. % Mn. It should be noted that the spectra of the 4 Mn and 12 Mn alloys with the form of a doublet, are well decomposed into spectra with an effective field at the iron nucleus $H_{\text{eff}}\approx6.8\times10^6$ A/m. In addition, the presence of a small part of a sextet with $H_{\text{eff}}\approx33.2\times10^6$ A/m is noted for the 4 Mn alloy, corresponding to sections of α-phase, which appear in the process of cold rolling in the preparation of the foils. However, alloys in the range from 6 to 10 at. % Mn show a singlet with a half-height width ω changing nonmonotonically as a function of concentration. This result is shown on the inset to Fig. 8. It can be seen that the maximum broadening of the spectra occurs for alloys with manganese content 5 and 10 at. %, which agrees with the critical concentrations $c_F=0.055$ and $c_{AF}=0.105$.

It is a feature of the singlets observed that they resist resolution into a sextet with a single effective field at the nucleus. For this a Gaussian distribution of H_{eff} must be assumed, within the limits $0-1.6\times10^7$ A/m. The magnetic state of the alloys containing from 6 to 10 at. % Mn can therefore with full justification be attributed to a spin glass with the existence of short-range ferro- and antiferromagnetic orders, and the most nonuniform spin glass is the alloy

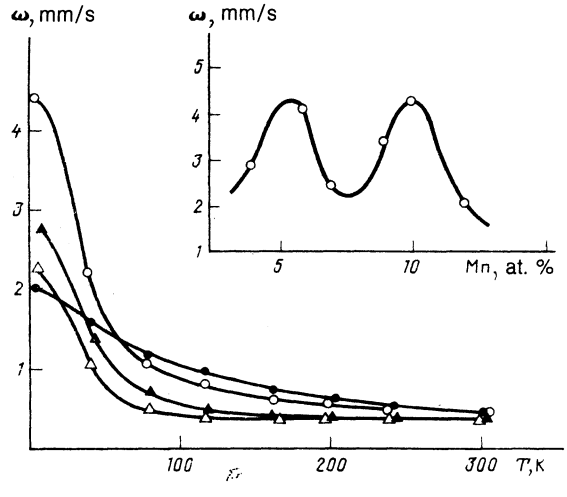

FIG. 8. Temperature dependence of Mössbauer line width at half height for $Fe_{0.7}Ni_{0.3-c}Mn_c$ alloys: ○) 10 Mn; ▲) 4 Mn; △) 7 Mn; ●) 12 Mn.

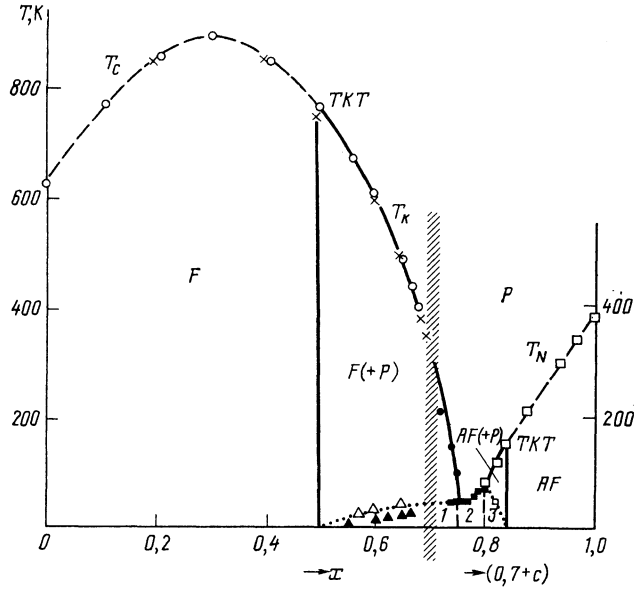

FIG. 9. Magnetic phase diagram of $Ni_{1-x}[Fe(Mn)]_x$ alloys. Dashed—second-order phase transition lines, full—first-order phase transition lines, the points separate the states of 1) reentrant ferromagnetic phase 2) spin glass and 3) antiferromagnetic reentrant phase; F and AF are respectively homogeneous ferromagnetic and antiferromagnetic, $F(+P)$ and $AF(+P)$ are respectively inhomogeneous (frustrated) ferromagnetism and antiferromagnetism, TKP is the tricritical point; □, ■, ● are the results of the present work; ○) Ref. 18, ×) Ref. 17, △) Ref. 3, ▲) Ref. 4.

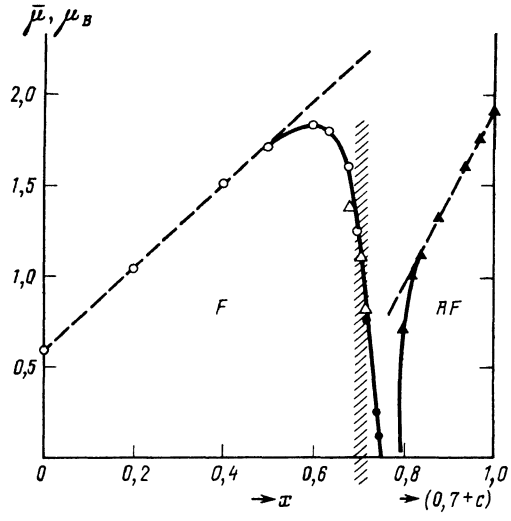

FIG. 10. Concentration dependence of the mean magnetic moment per atom of $Ni_{1-x}[Fe(Mn)]_x$ alloys: ▲, ● results of the present work; ○) Ref. 18; △) Ref. 17. The dashed lines denote the mixing law for $\bar{\mu}$.

7 Mn, which follows from the minimum value of the line width at half-maximum.

It was interesting to trace the change in line width with temperature. As would be expected, its strong increase in spin-glasses (Fig. 8) is observed at a temperature T_f which corresponds to the temperature of the paramagnet–spin glass transition.

Magnetic phase diagram. From the experimental results obtained the magnetic phase diagram of $Ni_{1-x}[Fe(Mn)]_x$ alloys can be constructed, which is shown in Fig. 9. It is put together from a combination of the phase diagrams of the alloys γ-$Ni_{1-x}Fe_x$ up to $x = 0.7$ and of the quasibinary solid solutions γ-$Fe_{0.7}Ni_{0.3-c}Mn_c$. Phase diagrams presented in this form can be considered as the prototype of complete magnetic phase diagrams of binary $A_{1-x}B_x$ alloys with fcc crystal symmetry for the magnetic atoms with competing exchange interaction of the type $J_{AA} > 0$, $J_{AB} > 0$ and $J_{BB} < 0$. In the present case nickel atoms appear as A and iron atoms as B in the ferromagnetic region and some averaged atoms (either iron or manganese) in the antiferromagnetic region.

The existence of the following regions is characteristic of such a phase diagram: 1) homogeneous ferromagnetism (F) and antiferromagnetism (AF); 2) frustrated ferromagnetism and antiferromagnetism coinciding with the region of tricritical behavior of the alloys, in which long-range magnetic order exists within the limits of the finite sized clusters with regions of quasiparamagnetic spin behavior; 3) spin-glass with the existence of ferromagnetic and antiferromagnetic correlations (cluster spin-glass).

We will characterize each of these states separately.

1) Homogeneous ferromagnetism and antiferromagnetism, characteristic of alloys with content 0–50 at. % Fe and 14–30 at. % Mn respectively, characterize the presence of long-range magnetic order over the whole region of a topologically unbounded cluster and the corresponding second-order phase transitions at the Curie, T_C, and Néel, T_N, temperatures. As follows from Fig. 10, the average magnetic moment in these regions changes linearly with concentration (shown by the dashed line), which reflects the constancy of the local magnetic moments on nickel, iron and manganese atoms.

In fact, for homogeneous ferromagnetism the concentration dependence of the mean magnetic moment $\bar{\mu}(x)$ is well described by the mixing law

$$\bar{\mu}(x) = \mu_{Ni}{}^{F}(1-x) + \mu_{Fe}{}^{F}x, \qquad (1)$$

where $\mu_{Ni}^{F} = 0.6\,\mu_B$ and $\mu_{Fe}^{F} = 2.8\,\mu_B$ are, respectively, the local magnetic moments of nickel and iron atoms in alloys with collinear ferromagnetic structure. In the case of homogeneous antiferromagnetism the mixing law can be written in the following way:

$$\bar{\mu}(c) = \mu_{Fe}{}^{AF}\cdot 0{,}7 + \mu_{Mn}{}^{AF}c + \mu_{Ni}{}^{AF}(0{,}3-c). \qquad (2)$$

Here μ_{Fe}^{AF}, μ_{Mn}^{AF} and μ_{Ni}^{AF} are, respectively, the local magnetic moments of iron, manganese and nickel atoms with collinear antiferromagnetic structure. To determine the values of these magnetic moments three independent equations are required. However, there are only two at our disposal:

$$d\bar{\mu}/dc = \mu_{Mn}{}^{AF} - \mu_{Ni}{}^{AF} = 5\mu_B, \qquad \mu_{Fe}{}^{AF}\cdot 0{,}7 + \mu_{Mn}{}^{AF}\cdot 0{,}3 = 1{,}9\mu_B.$$

Therefore we can assume certain possible variants of the distribution of magnetic moments within the limits of the concentration of the components at which the mixing law is satisfied for $\bar{\mu}(c)$. a) The magnetic moment of nickel atoms is directed parallel to the magnetic moment of the manganese and iron atoms in the antiferromagnetic sublattice, and its magnitude stays the same as in the ferromagnetic state, i.e. within the limits 0.6–1 μ_B, as follows from experiments on diffuse neutron scattering.[10] The magnetic moment of manganese atoms then becomes greater than 5 μ_B, which is impossible for the reason that its spin cannot exceed $S = 5/2$. b) The local magnetic moment of nickel atoms is, in general, absent for antiferromagnetic ordering of the

atomic spins of iron and manganese in the fcc lattice. In this situation $\mu_{Mn}^{AF} = 5\ \mu_B$ and $\mu_{Fe}^{AF} = 0.6\ \mu_B$, which is possible if it is not considered that 5 μ_B is too large a magnetic moment for manganese atoms in a metallic alloy. c) The local magnetic moment of nickel atoms is in the opposite direction relative to the iron and manganese moments in the antiferromagnetic sublattice because in this composition region an inversion from plus to minus has taken place in the sign of the exchange integrals J_{NiFe} and J_{NiMn}. Then, assuming that the value of μ_{Ni}^{AF} is not more than 1 μ_B, we obtain the values $\mu_{Mn}^{AF} \approx 4\ \mu_B$ and $\mu_{Fe}^{AF} \approx 1\ \mu_B$. Such magnitudes of the magnetic moments of iron and manganese atoms seem more realistic. But it is then important to note that, as in the previous case, μ_{Fe}^{AF} does not exceed 1 μ_B, which is appreciably different from the magnitude of the local moment of iron atoms in the ferromagnetic state, $\mu_{Fe}^{F} = 2.8\ \mu_B$. This result agrees fairly well with what is deduced from experimental[11,12] and theoretical[13] work in which the magnitude of the magnetic moment of iron in the γ-phase is assumed to be less than 1 μ_B.

2) The regions of inhomogeneous (frustrated) ferromagnetism and antiferromagnetism are bounded in the phase diagram (see Fig. 9) by two lines of first order phase transitions. The absence of a topologically unbounded magnetic cluster is characteristic of them and the ferromagnetic and antiferromagnetic order in these alloys exists only in the limits of finite clusters of a certain effective dimension L. Such a state is, on the one hand, a result of the accumulation of a number of antiferromagnetically interacting iron atoms with a ferromagnetic matrix of nickel atoms, and on the other hand of the existence of ferromagnetic interactions of nickel atoms in an antiferromagnetic matrix of iron and manganese atoms. Iron atoms for ferromagnetism and nickel atoms for antiferromagnetism play the role of sources of random magnetic fields,[14] leading to the instability of a topologically unbounded magnetic cluster and its division into regions of finite dimensions.

This means in thermodynamic language that for a certain concentration a point appears on the second order phase transition line, called the tricritical point (TCP), where the second-order phase transition changes to a first-order phase transition at the temperature T_K. On the temperature–concentration diagram a two-phase region appears, which represents the coexistence of a phase with order parameters of high symmetry and low symmetry. At the same time it is known, from the theory of phase transitions in systems with interacting order parameters, that the formation of a TCP is the result of strong coupling between the vector and scalar order parameters and weak coupling between the vector order parameters.[15]

In fact, according to Landau,[15] Gufar and Larin,[16] and Menshikov,[17] the thermodynamic potential Φ of a system having some coupled order parameters is described in general form in the following way:

$$\Phi = \Phi_0 + {}^1/_2 A_1 \mathbf{m}^2 + {}^1/_4 C_1 \mathbf{m}^4 + {}^1/_6 E_1 \mathbf{m}^6 + {}^1/_2 A_2 \mathbf{l}^2 + {}^1/_4 C_2 \mathbf{l}^4 + {}^1/_2 A_3 u^2 + {}^1/_2 A_4 v^2 + \lambda \mathbf{m}^2 \mathbf{l}^2 + \gamma \mathbf{m}^2 u + \varepsilon \mathbf{l}^2 v, \quad (3)$$

where in our case $\mathbf{m} = \mathbf{M}_1 + \mathbf{M}_2$ is the ferromagnetism vector, $\mathbf{l} = \mathbf{M}_1 - \mathbf{M}_2$ is the antiferromagnetism vector, $\mathbf{M}_1$ and $\mathbf{M}_2$ are the magnetization of the two chosen sublattices, u and v are the scalar order parameters which correspond, respectively, to vector ferromagnetic $\mathbf{m}$ and antiferromagnetic $\mathbf{l}$ order parameters and are characterized by the constants γ and ε of the magneto-elastic interaction. In addition, λ is the interaction constant of the vector order parameters and $C_1 > 0$, $C_2 > 0$, $E_1 > 0$, $A_3 > 0$, $A_4 > 0$.

Because of the existence of a weak interaction between the vector order parameters, we can take $\lambda = 0$. This means that the general potential decomposes into two independent parts, each of which after corresponding renormalization of the coefficients ($C_1^* = C_1 - 2\gamma/A_3$ and $C_2^* = C_2 - 2\varepsilon/A_4$) and for sufficiently large values of γ and ε, leads to negative values of C_1^* and C_2^*. This is the necessary condition for the existence of a TCP on the temperature-concentration phase diagram. The region of tricritical behavior in this case corresponds to a mixture of two phases, magnetically ordered and paramagnetic. We call such a state inhomogeneous or frustrated.

3) The spin-glass state of alloys on the phase diagram discussed in the composition region 5.5 Mn–10.5 Mn is characterized by the temperature T_f of the transition to the paramagnetic state which, as is seen from Fig. 9 for the "ferromagnetic spin-glass," is somewhat less than for the "antiferromagnetic." This is primarily associated with the fact that the spin-glass has a cluster character and the value of the exchange energy in antiferromagnetic clusters is larger than in ferromagnetic because of the presence of a large number of manganese atoms which, because of the conditions $\mu_{Mn}^{AF} > \mu_{Mn}^{AF}$ and $|J_{MnMn}| > |J_{FeFe}|$, produces a large exchange energy in the clusters.

CONCLUSIONS

The magnetic phase diagram of $Ni_{1-x}[Fe(Mn)]_x$ alloys presented here as the final result of the investigations, although not an exact representation of the phase diagram of $Ni_{1-x}Fe_x$ binary alloys with a fcc lattice, is nevertheless typical for binary $A_{1-x}B_x$ alloys with competing exchange interactions of the type $J_{AA} > 0$, $J_{AB} > 0$ and $J_{BB} < 0$. A characteristic feature of such phase diagrams is the existence of two tricritical points separating regions of homogeneous and inhomogeneous (frustrated) magnetism. From the thermodynamic point of view the latter is a mixture of magnetically ordered and paramagnetic phases. However, this state is in actual fact considerably more complicated. The magnetic order in such materials is achieved not in a topologically unbounded cluster, but in clusters of finite, but fairly large dimensions at the boundaries of which are regions of frustrated spins. These spins are not free as in a homogeneous paramagnet. They can therefore be assigned to the slowly relaxing category, which is the reason for the so-called hidden excitations.[5] In addition, below some temperature T_f the regions of slowly relaxing spins (or the paramagnetic phase in accordance with thermodynamics) transform into the spin-glass state, thus forming a mixed state of ordered and spin-glass phases, which is called a reentrant phase. Moreover, just the alloys with a region of tricritical behavior have a different kind of anomalous physical properties, to which belong the anomalously low values of the linear expansion coefficient and the temperature coefficient of the elastic modulus corresponding to Invar and Elinvar alloys.

Yet another distinguishing feature of such magnetic phase diagrams is the existence of a spin glass in the region of

compositions intermediate between ferromagnetic and antiferromagnetic. Such phase diagrams are a sign of the absence in the magnetic system of interaction between the vector order parameters and an indication of the existence of strong interaction between the vector and scalar order parameters, which is equivalent to a strong magneto-elastic interaction. The nature of the scalar order parameter (latent) can be different. In the case of $Ni_{1-x}Fe_x$ alloys its appearance is due to a reduction in the crystal volume and statistical fluctuations of the iron atoms surrounded only by iron atoms, where as a result of antiferromagnetic interaction between iron atoms, local reorientation of the spins takes place and a reduction in the partial magnetic moment of iron atoms from 2.8 μ_B to 1 μ_B. This is the main feature of Invar alloys.

The authors express their gratitude to L. V. Smirnov for preparing the alloys and to Yu. N. Skryabin for discussions of this work.

[1] M. Hatherly, K. Hirakawa, R. D. Lowde, J. F. Mallett, M. W. Stringfellow, and B. H. Torrie, Proc. Phys. Soc. London **84**, 55 (1964).
[2] A. Z. Men'shikov, N. N. Kuz'min, S. K. Sidorov, and Yu. A. Dorofeev, Fiz. Tverd. Tela (Leningrad) **16**, 3347 (1974) [Sov. Phys. Solid State **16**, 2171 (1974)].
[3] J. Miyazaki, Y. Ando, and M. Takahashi, J. Appl. Phys. **57**, 3456 (1985).
[4] H. Maruyama, R. Pauthenet, J-C. Picoche, and O. Yamada, J. Phys. Soc. Jpn. **55**, 3218 (1986).
[5] A. Z. Menshikov, Physica (Utrecht) B **161**, 1 (1989).
[6] Y. Nakamura, M. Hayase, M. Shiga, Y. Miyamoto, and N. Kawai, J. Phys. Soc. Jpn. **30**, 720 (1971).
[7] A. Z. Menchikov, A. Chamberod, and J. L. Tholence, Solid State Commun. **51**, 433 (1984).
[8] H. Umebayashi and Y. Ishikawa, J. Phys. Soc. Jpn. **21**, 1281 (1966).
[9] A. Z. Menshikov, V. A. Kazantsev, N. N. Kuzmin and S. K. Sidorov, J. Magn. Magn. Mater. **1**, 91 (1975).
[10] A. Z. Men'shikov, S. K. Sidorov, and V. E. Arkhipov, Zh. Eksp. Teor. Fiz. **61**, 311 (1971) [Sov. Phys. JETP **34**, 163 (1972)].
[11] L. Kaufman, E. V. Clougherty, and R. J. Weiss, Acta Metall. **11**, 323 (1963).
[12] S. C. Abrahams, L. Guttman, and J. S. Kasper, Phys. Rev. **127**, 2052 (1962).
[13] J. Kübler, Phys. Lett. A **81**, 81 (1981).
[14] Y. Imry and S-k Ma, Phys. Rev. Lett. **35**, 1399 (1975).
[15] L. D. Landau, Zh. Eksp. Teor. Fiz. **7**, 19 (1937).
[16] Yu. M. Gufan and E. S. Larin, Fiz. Tverd. Tela (Leningrad) **22**, 463 (1980) [Sov. Phys. Solid State **22**, 270 (1980)].
[17] A. Z. Menshikov, Physica B **149**, 249 (1988).
[18] J. Crangle and G. C. Hallam, Proc. R. Soc. London A **272**, 119 (1963).

Translated by R. Berman